Bridging Hydride at Reduced H-Cluster Species in [FeFe]-Hydrogenases Revealed by Infrared Spectroscopy, Isotope Editing, and Quantum Chemistry

Stefan Mebs[†]*, Moritz Senger[‡], Jifu Duan[#], Florian Wittkamp[§], Ulf-Peter Apfel[§], Thomas Happe[#], Martin Winkler[#], Sven T. Stripp[‡]*, and Michael Haumann[†]*

[†]Department of Physics, Biophysics of Metalloenzymes, Freie Universität Berlin, 14195 Berlin, Germany

[‡]Department of Physics, Experimental Molecular Biophysics, Freie Universität Berlin, 14195 Berlin, Germany

[#]Faculty of Biology and Biotechnology, Photobiotechnology, Ruhr-Universität Bochum, 44801 Bochum, Germany

[§]Faculty of Chemistry and Biochemistry, Bioinorganic Chemistry, Ruhr-Universität Bochum, 44801 Bochum, Germany

ABSTRACT: [FeFe]-Hydrogenases contain a H_2-converting cofactor (H-cluster) in which a canonical [4Fe-4S] cluster is linked to a unique diiron site with three carbon monoxide (CO) and two cyanide (CN^-) ligands (e.g. in the oxidized state, **Hox**). There has been much debate whether reduction and hydrogen binding may result in alternative rotamer structures of the diiron site in a single (**Hred**) or double (**Hsred**) reduced H-cluster species. We employed infrared spectro-electrochemistry and site-selective isotope editing to monitor the CO/CN^- stretching vibrations in [FeFe]-hydrogenase HYDA1 from *Chlamydomonas reinhardtii*. Density functional theory calculations yielded vibrational modes of the diatomic ligands for conceivable H-cluster structures. Correlation analysis of experimental and computational IR spectra has facilitated an assignment of **Hred** and **Hsred** to structures with a bridging hydride at the diiron site. Pronounced ligand rotation during μH binding seems to exclude **Hred** and **Hsred** as catalytic intermediates. Only states with a conservative H-cluster geometry featuring a μCO ligand are likely involved in rapid H_2 turnover.

Hydrogenases are the most efficient biological catalysts for hydrogen (H_2) formation and oxidation, making them relevant for renewable fuel technology and catalysis research.[1] Figure 1 shows the active site cofactor (H-cluster) in a crystallized [FeFe]-hydrogenase,[2,3] comprising a [4Fe-4S] cluster linked via a cysteine to a unique diiron site, [2Fe]. In the "active-ready" oxidized state (**Hox**), the iron atoms in proximal (Fe_p) or distal (Fe_d) position relative to the [4Fe-4S] cluster each carry one terminal CO and CN^- ligand.[4] Fe_p and Fe_d are interconnected by a bridging carbonyl (μCO) and an aminodithiolate (adt, $(SCH_2)_2NH$).[5,6] Fe_d shows a vacant coordination site.[3] The adjacent adt nitrogen base and a conserved cysteine presumably serve as proton relays in the catalytic cycle.[7] Putative hydrogen bonds between the protein scaffold and the CN^- ligands involve Ser232 and Lys358.[8]

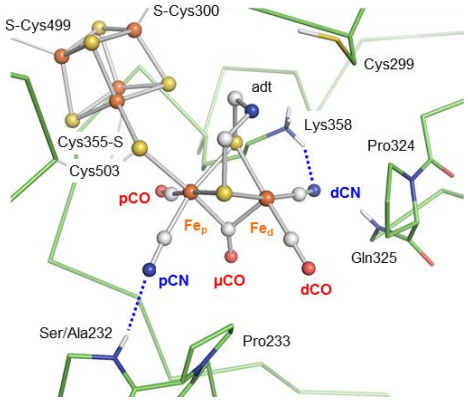

Figure 1. Crystal **s**tructure of the H-cluster in bacterial [FeFe]-hydrogenase (CpI, PDB entry 4XDC).[2] Dashes mark putative H-bonds. Ser232 in CpI is Ala in HYDA1, Lys358 and Cys299 are conserved residues, the N(adt) proton is omitted.

In the last decades, a variety of intermediate states of the H-cluster has been characterized (see, e.g., refs.[7,9-23]). However, the chemical nature and the role of many species in the catalytic cycle have remained elusive. In this study, we focus on single or double ("super-") reduced species,[7] which carry one (**Hred**, **Hred′**) or two (**Hsred**, **Hhyd**) surplus electrons relative to **Hox**. Recently, **Hred′** was assigned to a structure with a μCO and an apical vacancy,[9,24] as well as a proton at a cysteine ligand of the [4Fe-4S] cluster.[24] For **Hhyd**, a μCO and an apical hydride at Fe_d were assigned.[10,12,22,25,26] For **Hred** and **Hsred**, several structural isomers have been suggested, differing with respect to the metal-bridging ligand and to the location of protons at the diiron site.[9,11,13,15-17,27] Three basic model types for **Hred** and **Hsred** can be distinguished: (**I**) Structures with a μCO ligand and a proton (i.e. a formal hydride) or H_2 bound at Fe_d (Figs. 2a, S5). (**II**) Structures with an

open metal-bridging site, a vacancy at Fe_d, and additional protonation at the N(adt) (Fig. 2b). (**III**) Structures with a bridging hydride (μH) or ηH_2 (Figs. 2c, S5).

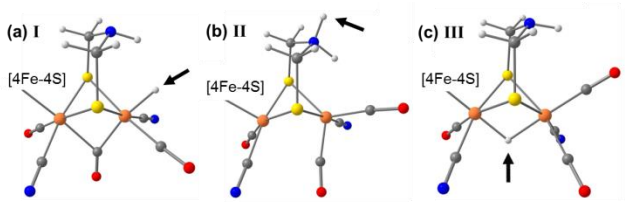

Figure 2. Basic diiron site structures for **Hred** and **Hsred**. Structural variants for DFT were designed following literature proposals[10-13,15-17] (Fe, orange; S, yellow; O, red; N, blue; C, gray; H, light-gray; [4Fe-4S] cluster abbreviated for clarity). See Fig. S5 for complete and further structures (e.g. with CO/CN^- rotation or a H_2 ligand). Arrows mark H^+ binding.

We have recently demonstrated that the combination of attenuated total reflection Fourier-transform infrared spectroscopy (ATR-FTIR) with density functional theory (DFT) is powerful for structural elucidation of the H-cluster.[14,24,25] The CO/CN^- vibrations are specific markers of changes in geometric and electronic configuration in response to redox and protonation reactions, as well as of ligand binding. Selective ^{13}CO editing leads to characteristic IR-frequency shifts that serve as benchmarks for DFT.[14] However, modelling of structural and electronic changes in reduced states requires consideration of 'internal' isomerism (rotamers), as observed for CO binding at [2Fe] (**Hox-CO**),[14] the influence of hydrogen bonding,[2,8] variation of protonation sites,[24,25,28] and effects related to the theory level,[20,29] which were here addressed to determine the chemical nature of **Hred** and **Hsred**.

Chlamydomonas reinhardtii [FeFe]-hydrogenase HYDA1 was purified and activated,[5,30] and ^{13}CO editing at [2Fe] was achieved as reported earlier.[14] A novel ATR-FTIR set-up for spectro-electrochemistry (Fig. S1) facilitated selective population of redox states of the H-cluster (Fig. S2). CO/CN^- band frequencies and intensities were derived from experimental IR spectra using a global fit approach (Fig. S3). In DFT calculations (Gaussian09), based on the CpI structure,[2] model variants **I-III** were generated (Figs. 2, S5) and assignment of anti-ferromagnetic coupling (broken symmetry approach) was followed by geometry optimization. Larger models containing Ala232 or Ala232 and Lys358 (Figs. 1, S5), ^{13}CO editing, and DFT functional (BP86 or TPSSh) and dielectric constant (COSMO solvation model) variations were considered. Normal mode analysis yielded the theoretical CO/CN^- vibrations.

The experimental IR spectra of **Hox**, **Hred**, **Hred′**, and **Hsred** are compared in Fig. 3. The well-known CO/CN^- band pattern of **Hox** agrees with an apical vacancy at Fe_d and a μCO ligand.[14] The similar spectrum of **Hred′** is assigned to a structure with a reduced [4Fe-4S] cluster, a μCO, and apical vacancy as in **Hox**.[9,24] **Hred** and **Hsred** show IR patterns with pronounced CO/CN^- band shifts and relative intensity changes vs. **Hox**. A ~90 cm^{-1} up-shift of the CO band α, due to μCO in **Hox**, down-shifts of the other CO/CN^- bands, and intensity reversal of the CO bands α and β suggested significant structural changes at the diiron site. A doubled frequency difference of the two CN^- bands (~40 cm^{-1} in **Hred** and **Hsred** vs. ~20 cm^{-1} in **Hox**) was observed.[11,27] ^{13}CO isotope editing and H/D exchange experiments revealed similar CO band frequency shifts for **Hred** and **Hsred** (Fig. S4, Table S1). These results indicated that both states adopt a similar geometry of the H-cluster, which differs from **Hox**. Structural isomerism (ligand rotation) seems not to occur in the **Hred** to **Hsred** reduction, as in the **Hox** to **Hred′** reduction.[9,24]

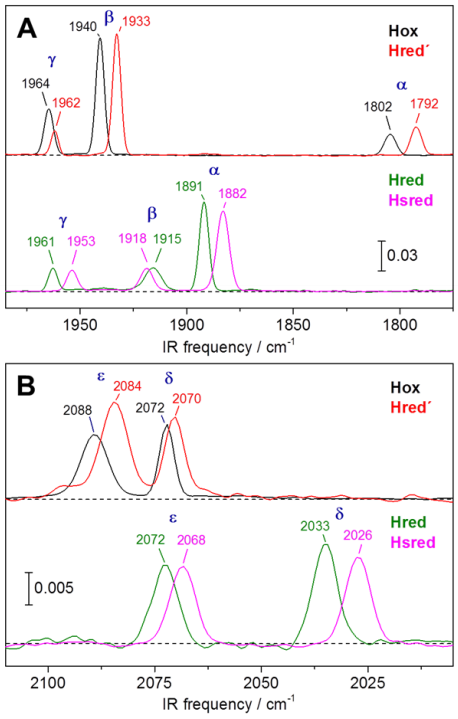

Figure 3. Experimental ATR-FTIR spectra of HYDA1. (A) CO ligand region. (B) CN^- ligand region. Band frequencies (in cm^{-1}) were derived from fit analysis. Spectra were recorded at -200 mV (**Hox**), -400 mV (**Hred**), -750 mV (**Hred′**), or -900 mV (**Hsred**) vs. SHE using a spectro-electrochemical set-up (Fig. S1), background and minor species contributions were subtracted (Fig. S2), and spectra were normalized (Fig. S3).

DFT calculations were carried out on model types **I**-**III** of **Hred** and **Hsred** (Figs. 2, S5). The theoretical IR spectra revealed that the coupling of the CO stretching vibrations strongly differs between the model types, meaning that the CO bands (α, β, γ) were attributable to different vibrational modes (see SI and Fig. S6 for a detailed analysis). Comparable effects were observed for rotational isomers (e.g. equatorial vs. apical CN^- at Fe_d) and ^{13}CO isotopomers. Linear fits to data in plots of calculated vs. experimental IR frequencies (F) for **Hred** and **Hsred** structures revealed variable CO/CN^- F-offsets and deviations from an ideal slope of unity, depending on the DFT functional and dielectric constant, redox state, and structure type/size (Fig. S7). Alignment of calculated and experimental IR spectra using a common offset/slope correction, which works for species with a similar [2Fe] geometry (i.e. **Hox**, **Hred′**),[14,24,25] thus was inadequate for comparing **Hred** and **Hsred** with **Hox**. We used individual F-offset corrections (i.e. the same F-shift for all CO/CN^- bands, neglecting slope deviations) as a least biased evaluation approach, which facilitated a statistical correlation of experimental and calculated CO/CN^- frequencies of **Hred** and **Hsred** using the root-mean-square deviation (Eq. 1; n = 5 CO/CN^- ligands, $F^{cor} = F^{cal} - F^{offset}$):

$$rmsd = \sqrt{\sum \left(F_i^{\exp} - F_i^{cor}\right)^2 / n} \quad . \tag{1}$$

Tables S2-S6 summarize calculated IR frequencies and intensities, F-shifts, and rmsd values for all calculated models. Linear fits to calculated vs. experimental CO/CN^- frequencies and frequency differences yielded R^2-factors as a further quality criterion (Tables S7, S8; Fig. S9).

Figure 4 shows a correlation plot of calculated frequencies for **Hred** and **Hsred** model types **I**-**III** vs. experimental frequencies. The frequencies for type **III** models (μH) are in best agreement with the experimental data (see also Figs. S7, S8). The small rmsd for models lacking amino acids was in the range of 13-25 cm^{-1} for all six type **III** rotamers, whereas an at least 2-fold larger rmsd (34-67 cm^{-1} or 25-57 cm^{-1}) was obtained for models **I** or **II** (Tables S2, S3). Inclusion of Ala232 or Ala232/Lys358 improved the rmsd of all models, so that type **III** remained superior. Protonation at a cysteine ligand of the [4Fe-4S] cluster[24,25] in model **III** of **Hsred** (μH) shifted the CO/CN^- bands by <3 cm^{-1} on average. The linear regression parameters supported that models with a μH represent the best description of **Hred** and **Hsred** (Tables S7, S8). Variation of the DFT functional or dielectric constant had a considerable effect on the rmsd values, but models with a μH were favored at all theory levels (Table S5).

Discrimination of the actual rotamer structure of **Hred** and **Hsred** required in-depth analysis of the DFT data. Lowest rmsd values were obtained for type **III** structures with an apical CO or CN^- at Fe_d. Type **III** rotamers with p/dCO/CN^- ligand inversion or pCO/CN^- inversion and an apical CN^- at Fe_d were disfavored by their larger rmsd (Tables S2, S3, S6). Trans-axial effects between bridging and apical ligands and hydrogen bonding of N(adt) also affect the rmsd. For example in models **II** of **Hred** and **Hsred**, the 2-fold diminished rmsd for apical CN^- vs. CO is due to the dCN$^-$-HN(adt) interaction, resulting in rotation of the semi-bridging CO (Fig. S5) and in p/dCN$^-$ vibrational decoupling (as in model **III**).

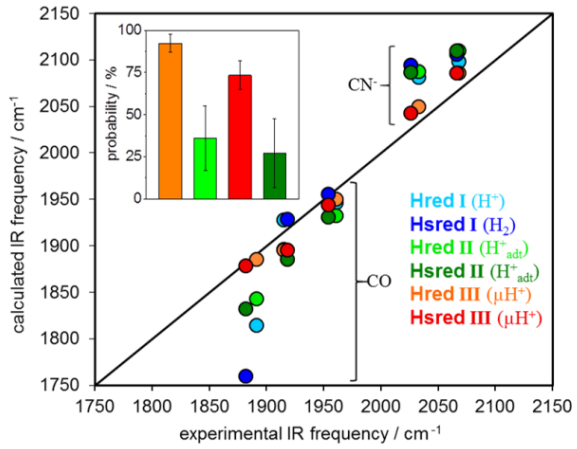

Figure 4. Comparison of calculated and experimental CO/CN^- frequencies. DFT data (TPSSh, ε = 4) refers to indicated structures (containing Ala232; Figs. 2, S5). Computational and experimental frequencies were aligned (Tables S2, S3). Inset: "probability" of selected structures (see Table S11).

^{13}CO editing provided further insight into the rotamer structure (Tables S1, S6, Fig. S9). Pronounced shifts of CO band β in models **II** (protonation at N(adt), open bridge) with an apical CO at Fe_d for **Hred** and **Hsred** disfavored such structures. More equal shifts of all three CO bands in models **II** and **III** with an apical CN^- at Fe_d for all ^{13}CO labeling patterns also disagreed with experimental data. Only models **III** (μH) with an apical CO at Fe_d of **Hred** and **Hsred** reproduced the experimental ^{13}CO band shifts reasonably well, which suggested equatorial CO and CN^- ligands at Fe_d as in **Hox**. Two further features of the experimental **Hred** and **Hsred** IR spectra were well described only by models **III** (μH) with an apical CO (Fig. S8): (i) The large frequency gap of the CN^- ligands (29-44 cm^{-1}), in contrast to an about 2-fold smaller gap for an apical CN^-. (ii) The large intensity increase of the CO band α, which remains weak for an apical CN^-. An analysis of the electronic

configuration of the **Hred** and **Hsred** structures with a bridging hydride is provided in the SI. For **Hox** and **Hred′**, H-bonding amino acids in the DFT structures have no decisive effect on the IR bands.[14,24,25] For **Hred** and **Hsred** models **III**, inclusion of Ala232 or Ala232/Lys358 yielded significant CN^- frequency down-shifts (≤10 cm^{-1}), leading to improved agreement with the experimental data (Table S4). H-bonding seemingly has a more significant effect on the electron density distribution in the H-cluster with a reduced rather than oxidized diiron site.

In this study, the combination of ATR-FTIR, ^{13}CO editing, and DFT has yielded a structural assignment of the **Hred** and **Hsred** states of the H-cluster. Our analysis favors a one- or two-electron reduced structure for **Hred** and **Hsred**, both carrying a bridging hydride and an apical CO ligand at the diiron site (Table S11). **Hox** has been assigned to a (formal) $[4Fe\text{-}4S]^{2+}$-$[Fe^{II}Fe^{I}]$ complex[16,31] and **Hred′** represents a $[H^+4Fe\text{-}4S]^{1+}$-$[Fe^{II}Fe^{I}]$ complex,[9,24] both with a μCO ligand and an apical vacancy.[2] Here, we assign **Hred** to a (formal) $[4Fe\text{-}4S]^{2+}$-$Fe^{II}(\mu H^-)Fe^{II}$] complex and **Hsred** to a $[4Fe\text{-}4S]^{1+}$-$Fe^{II}(\mu H^-)Fe^{II}$] complex.[16] Protonation at the [4Fe-4S] cluster besides of the μH in **Hsred** is not excluded. Reversible **Hred** and **Hsred** formation[32] seems to be compatible with a μH because ligand rotation at the H-cluster upon hydride binding/removal may readily occur on the minutes timescale of typical spectroscopic experiments on enzymes in solution. Pronounced ligand rotation at the diiron site during μH binding implies that **Hred** and **Hsred** are unlikely catalytic intermediates during sustained H_2 conversion.[33,34]

HYDA1 is located in the stroma of the algal chloroplast.[35] However, **Hred** and **Hsred** seem to accumulate preferentially at acidic pH.[11,22,24] Such a pH may favor faster protonation at the diiron site than at the [4Fe-4S] cluster, which biases the first surplus electron to the diiron site and facilitates μH binding.[24,25] More rapid [4Fe-4S] cluster protonation, i.e. at physiological alkaline pH, locates the first electron at the cubane and likely prevents ligand rotation and μH binding. These considerations suggest that only states with a conservative diiron site geometry (i.e. **Hox**, **Hred′**, **Hhyd**) are involved in the rapid H_2 turnover of [FeFe]-hydrogenases.

ASSOCIATED CONTENT

Supporting Information

ATR-FTIR spectro-electrochemistry methods, computational structures and IR data evaluation, electronic structure analysis (file type PDF). The Supporting Information is available free of charge on the ACS Publications website.

AUTHOR INFORMATION

Corresponding Authors

*stefan.mebs@fu-berlin.de

*sven.stripp@fu-berlin.de

*michael.haumann@fu-berlin.de

Notes

The authors declare no competing financial interests.

ACKNOWLEDGMENTS

We thank the BMBF (Grant 05K14KE1 to M.H.), the VW Foundation (Grant LigH2t to T.H.), the DFG (RESOLV, EXC1069; Emmy Noether Grant AP242/2-1 to U.-P.A.), and the Fonds der Chemischen Industrie (Liebig Grant to U.-P.A.) for funding. M.S. and S.T.S. thank the International Max Planck Research School on Multiscale Biosystems and the Focus Area NanoScale (FU-Berlin) for financial support.

REFERENCES

(1) Abbasi, T.; Abbasi, S. A. *Renew. Sustain. Energy Rev.* **2011**, *15*, 3034.

(2) Esselborn, J.; Muraki, N.; Klein, K.; Engelbrecht, V.; Metzler-Nolte, N.; Apfel, U.-P.; Hofmann, E.; Kurisu, G.; Happe, T. *Chem. Sci.* **2016**, *7*, 959.

(3) Peters, J. W.; Lanzilotta, W. N.; Lemon, B. J.; Seefeldt, L. C. *Science* **1998**, *282*, 1853.

(4) Pierik, A. J.; Hulstein, M.; Hagen, W. R.; Albracht, S. P. *Eur. J. Biochem.* **1998**, *258*, 572.

(5) Esselborn, J.; Lambertz, C.; Adamska-Venkatesh, A.; Simmons, T.; Berggren, G.; Noth, J.; Siebel, J.; Hemschemeier, A.; Artero, V.; Reijerse, E.; Fontecave, M.; Lubitz, W.; Happe, T. *Nat. Chem. Biol.* **2013**, *10*, 607.

(6) Berggren, G.; Adamska, A.; Lambertz, C.; Simmons, T. R.; Esselborn, J.; Atta, M.; Gambarelli, S.; Mouesca, J. M.; Reijerse, E.; Lubitz, W.; Happe, T.; Artero, V.; Fontecave, M. *Nature* **2013**, *499*, 66.

(7) Lubitz, W.; Ogata, H.; Rudiger, O.; Reijerse, E. *Chem. Rev.* **2014**, *114*, 4081.

(8) Winkler, M.; Esselborn, J.; Happe, T. *Biochim. Biophys. Acta* **2013**, *1827*, 974.

(9) Sommer, C.; Adamska-Venkatesh, A.; Pawlak, K.; Birrell, J. A.; Rudiger, O.; Reijerse, E. J.; Lubitz, W. *J. Am. Chem. Soc.* **2017**, *139*, 1440.

(10) Reijerse, E. J.; Pham, C. C.; Pelmenschikov, V.; Gilbert-Wilson, R.; Adamska-Venkatesh, A.; Siebel, J. F.; Gee, L. B.; Yoda, Y.; Tamasaku, K.; Lubitz, W.; Rauchfuss, T. B.; Cramer, S. P. *J. Am. Chem. Soc.* **2017**, *139*, 4306.

(11) Adamska, A.; Silakov, A.; Lambertz, C.; Rudiger, O.; Happe, T.; Reijerse, E.; Lubitz, W. *Angew. Chem. Int. Ed. Engl.* **2012**, *51*, 11458.

(12) Mulder, D. W.; Guo, Y.; Ratzloff, M. W.; King, P. W. *J. Am. Chem. Soc.* **2016**, *139*, 83.

(13) Mulder, D. W.; Ratzloff, M. W.; Bruschi, M.; Greco, C.; Koonce, E.; Peters, J. W.; King, P. W. *J. Am. Chem. Soc.* **2014**, *136*, 15394.

(14) Senger, M.; Mebs, S.; Duan, J.; Wittkamp, F.; Apfel, U. P.; Heberle, J.; Haumann, M.; Stripp, S. T. *Proc. Natl. Acad. Sci. U. S. A.* **2016**, *113*, 8454.

(15) Lambertz, C.; Chernev, P.; Klingan, K.; Leidel, N.; Siegfridsson, K. G. V.; Happe, T.; Haumann, M. *Chem. Sci.* **2014**, *5*, 1187.

(16) Chernev, P.; Lambertz, C.; Brunje, A.; Leidel, N.; Sigfridsson, K. G.; Kositzki, R.; Hsieh, C. H.; Yao, S.; Schiwon, R.; Driess, M.; Limberg, C.; Happe, T.; Haumann, M. *Inorg. Chem.* **2014**, *53*, 12164.

(17) Fourmond, V.; Greco, C.; Sybirna, K.; Baffert, C.; Wang, P. H.; Ezanno, P.; Montefiori, M.; Bruschi, M.; Meynial-Salles, I.; Soucaille, P.; Blumberger, J.; Bottin, H.; De Gioia, L.; Leger, C. *Nat. Chem.* **2014**, *6*, 336.

(18) Baffert, C.; Bertini, L.; Lautier, T.; Greco, C.; Sybirna, K.; Ezanno, P.; Etienne, E.; Soucaille, P.; Bertrand, P.; Bottin, H.; Meynial-Salles, I.; De Gioia, L.; Leger, C. *J. Am. Chem. Soc.* **2011**, *133*, 2096.

(19) Finkelmann, A. R.; Stiebritz, M. T.; Reiher, M. *Chem. Sci.* **2013**, *5*, 215.

(20) Yu, L.; Greco, C.; Bruschi, M.; Ryde, U.; De Gioia, L.; Reiher, M. *Inorg. Chem.* **2011**, *50*, 3888.

(21) Ryde, U.; Greco, C.; De Gioia, L. *J. Am. Chem. Soc.* **2010**, *132*, 4512.

(22) Winkler, M.; Senger, M.; Duan, J.; Esselborn, J.; Wittkamp, F.; Hofmann, E.; Apfel, U.-P.; Stripp, S. T.; Happe, T. *Nat. Commun.* **2017**, *16115*, doi:10.1038/ncomms16115.

(23) Bruschi, M.; Greco, C.; Fantucci, P.; De Gioia, L. *Inorg. Chem.* **2008**, *47*, 6056.

(24) Senger, M.; Mebs, S.; Duan, J.; Shulenina, O.; Laun, K.; Kertess, L.; Wittkamp, F.; Apfel, U.-P.; Happe, T.; Winkler, M.; Haumann, M.; Stripp, S. T. *Phys. Chem. Chem. Phys.* **2017**, *under review*.

(25) Mebs, S.; Kositzki, R.; Duan, J.; Senger, M.; Wittkamp, F.; Apfel, U.-P.; Happe, T.; Stripp, S. T.; Winkler, M.; Haumann, M. *Biochim. Biophys. Acta* **2017**, *under review*.

(26) Katz, S.; Noth, J.; Horch, M.; Shafaat, H. S.; Happe, T.; Hildebrandt, P.; Zebger, I. *Chem. Sci.* **2016**, *7*, 6746.

(27) Mulder, D. W.; Ratzloff, M. W.; Shepard, E. M.; Byer, A. S.; Noone, S. M.; Peters, J. W.; Broderick, J. B.; King, P. W. *J. Am. Chem. Soc.* **2013**, *135*, 6921.

(28) Noth, J.; Kositzki, R.; Klein, K.; Winkler, M.; Haumann, M.; Happe, T. *Sci. Rep.* **2015**, *5*, 1.

(29) Bruschi, M.; Greco, C.; Kaukonen, M.; Fantucci, P.; Ryde, U.; De Gioia, L. *Angew. Chem. Int. Ed. Engl.* **2009**, *48*, 3503.

(30) Noth, J.; Esselborn, J.; Guldenhaupt, J.; Brunje, A.; Sawyer, A.; Apfel, U. P.; Gerwert, K.; Hofmann, E.; Winkler, M.; Happe, T. *Angew. Chem. Int. Ed. Engl.* **2016**, 55, 8396.

(31) Kamp, C.; Silakov, A.; Winkler, M.; Reijerse, E. J.; Lubitz, W.; Happe, T. *Biochim. Biophys. Acta* **2008**, *1777*, 410.

(32) Roseboom, W.; De Lacey, A. L.; Fernandez, V. M.; Hatchikian, E. C.; Albracht, S. P. *J. Biol. Inorg. Chem.* **2006**, *11*, 102.

(33) Hajj, V.; Baffert, C.; Sybirna, K.; Meynial-Salles, I.; Soucaille, P.; Bottin, H.; Fourmond, V.; Leger, C. *Energy Environ. Sci.* **2014**, *7*, 715.

(34) Filippi, G.; Arrigoni, F.; Bertini, L.; De Gioia, L.; Zampella, G. *Inorg. Chem.* **2015**, *54*, 9529.

(35) Stripp, S. T.; Happe, T. *Dalton Trans.* **2009**, 9960.